IChemE

www.icheme.org/cherd
doi: 10.1205/cherd05044

0263–8762/06/$30.00+0.00
© 2006 Institution of Chemical Engineers
Trans IChemE, Part A, August 2006
Chemical Engineering Research and Design, 84(A8): 691–702

PERFORMANCE OPTIMIZATIONS OF GRID DISC IMPELLERS FOR MIXING OF SINGLE-PHASE FLOWS IN A STIRRED VESSEL

A. DEWAN[†], V. BUWA[*] and F. DURST

Lehrstuhl für Strömungsmechanik (LSTM), Friedrich-Alexander-Universität Erlangen-Nürnberg, Erlangen, Germany

This paper reports numerical investigations performed to optimize the mixing performance of a radial grid disc impeller in a stirred vessel. In the author's previous work (Buwa *et al.*, 2006, *Chem Eng Sci*, 61: 2815–2822), a novel grid disc impeller having radial flow characteristics was developed, numerical simulations of the flow generated by the grid disc impeller were performed and the predictions were validated experimentally. In the present work, the numerical simulations were performed to investigate the effects of the rotational speed, grid opening size and impeller diameter on the mean flow generated by the various impeller configurations, mixing performance and power requirements. Numerical simulations were also carried out to evaluate the performance of a dual radial grid disc impeller. The results show that the mixing efficiency per unit power consumed improves with an increase in the grid opening size and also with an increase in the diameter of the grid disc impeller. Further, the mixing efficiency was significantly improved for the dual grid disc impeller with large grid openings.

Keywords: stirred vessel; grid disc impeller; single-phase flow; mixing; power consumption; numerical simulations.

INTRODUCTION

A large number of process applications, for example in the chemical, biochemical, mineral and wastewater processing industries, employ stirred vessels. The mixing of single-phase flow is an important process in such vessels. The energy requirements of a mixing process constitute a major expenditure and, with the rising cost of energy, it is imperative that efforts are made to design profitable operational protocols. Because of the widespread applications of stirred vessels in the process industry, even a small reduction in the operational costs of these vessels can result in major cost savings. In the past, although several groups have attempted to improve the performance of different impellers in terms of their power consumption under consideration of pumping capacity and degree of mixing achieved, new types of impellers are continuously being developed and put forward for practical applications (see e.g., Mavros *et al.*, 2001; Li *et al.*, 2004).

In their previous work (Buwa *et al.*, 2006), the authors developed a novel grid disc impeller [Figure 1(a)]. They showed that this impeller has the radial flow characteristics and mixing efficiency per unit power consumed is as good as that of a propeller (which has the axial flow characteristics and is known to have good mixing efficiency per unit power consumed). In the present work, the effect of the grid opening size, impeller diameter and different impeller configurations was investigated numerically to improve the mixing efficiency of the radial grid impeller that the authors proposed in their previous work.

Mixing in a stirred vessel is achieved by three means, molecular motion, turbulent fluctuations and bulk convection (or circulation) of the fluid (Nere *et al.*, 2003). Hence the total mixing in a stirred vessel depends on the mean flow and turbulence, which in turn depends on the shape and size of the vessel and impeller and also the location of the impeller within the vessel. Depending on the process requirements, several different types of impellers are used in industry. These impellers are broadly classified as either radial (e.g., Rushton turbine) or axial (e.g., propeller and pitched blade turbine), depending on the direction of the secondary flow (the primary flow being the rotational flow in the direction of the impeller motion). In the open literature, the standard impellers have been widely investigated (see e.g., Derksen *et al.*, 1999; Lee and Yianneskis, 1998; Schafer *et al.*, 1998; Aubin *et al.*, 2001). All these studies show that the mixing in a stirred vessel is directly related to the nature of the secondary flow. Various parameters, such as the impeller shape, impeller diameter, number of impeller

[*]*Correspondence to*: Dr V. Buwa, Lehrstuhl für Strömungsmechanik (LSTM), Friedrich-Alexander-Universität Erlangen-Nürnberg, Cauerstraße 4, D-91058, Erlangen, Germany.
E-mail: vivek.buwa@lstm.uni-erlangen.de
[†]On leave from the Department of Mechanical Engineering, Indian Institute of Technology Guwahati, Guwahati, India.

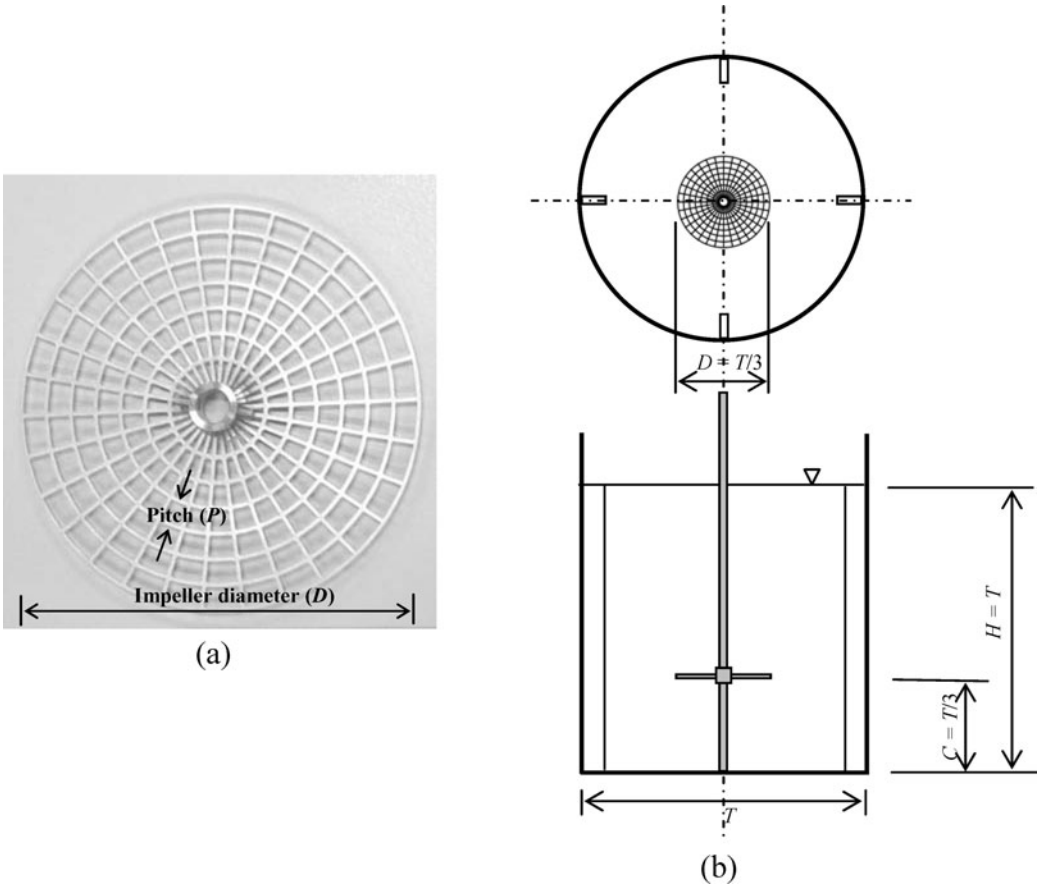


Figure 1. (a) A radial grid disc impeller developed by Buwa *et al.* (2006) and (b) stirred vessel configuration used in the present work.

blades, tank diameter and clearance of impeller from the tank bottom, significantly affect the flow behaviour and therefore the mixing characteristics in a stirred vessel (Kramers *et al.*, 1953; Li *et al.*, 2004; Micale *et al.*, 1999; Montante *et al.*, 2001a, b).

The flow generated by the rotating impeller interacts with the baffles mounted at the wall of the tank and results in a complex unsteady, three-dimensional and highly turbulent flow. Because of this complexity, the fluid flow in a stirred vessel remains difficult to understand. With continuous research efforts over the last decade, computational fluid dynamics (CFD) has now become an effective tool for the design of stirred vessels. One of the challenges to the numerical prediction of the flow in a stirred vessel is accurate prediction of the fluid turbulence. Numerical simulations of turbulent flows can be performed in three ways: (1) direct numerical simulations (DNS), (2) large eddy simulations (LES) and (3) simulations using the Reynolds-averaged Navier–Stokes (RANS) equations.

In the DNS, the equations for instantaneous flow are solved and therefore no modelling is required. Since all scales ranging from the smallest scales, where the dissipation of the turbulent kinetic energy into thermal energy takes place (termed as the Kolmogorov length scale), up to the largest scales (typically defined by the characteristic length of the flow problem) are resolved, DNS requires enormous computational efforts. Therefore, the DNS studies are still limited to the flow problems with very small Reynolds numbers and simple geometries. In the LES, as the name suggests, only the large scales are resolved and the smallest scales are modelled. This is because the large scale eddies are affected by the boundary conditions and therefore should be computed, but small scales are largely independent of the flow geometry, tend to be homogeneous and isotropic, and therefore can be easily modelled. Although the LES requires less computational efforts than that of the DNS, the computational requirements of the LES remain still high for the optimization of complicated process equipment where a large number of computations need to be performed.

In the RANS approach, the Reynolds-averaged Navier–Stokes (RANS) equations are solved to predict the mean flow properties. However, an appropriate turbulence model is needed to close the set of governing equations. This is the most widely used approach for practical engineering flows (see e.g., Khopkar *et al.*, 2004; Li *et al.*, 2004), mainly because it is computationally much less expensive than DNS and LES. Several different turbulence models have been developed to close the RANS equations, which include the simplest zero-equation model to the most complex Reynolds-stress transport models (RSTM). In a zero-equation model, no additional transport equation is employed and the closure is achieved by using algebraic relationships. Two additional transport equations are solved in the standard $k-\varepsilon$ model, namely for turbulent kinetic energy and its rate of dissipation. All these available eddy diffusivity models, ranging from the zero-equation models to two-equation models, use the simple Boussinesq

approximation, according to which the local Reynolds stress and local mean rate of strain are in equilibrium. In the RSTM, no such equilibrium is assumed and six transport equations for each component of Reynolds stress and one equation for the dissipation of turbulent kinetic energy are solved.

The standard $k-\varepsilon$ model of turbulence, which has been widely applied to study practical flows (e.g., Khopkar *et al.*, 2004), is known to be inaccurate for anisotropic turbulence and turbulent flow in the vicinity of solid walls. The use of low Reynolds number versions of the $k-\varepsilon$ model does not improve the predictions of turbulent flow in stirred vessels (Jones *et al.*, 2001). Jenne and Reuss (1999) and Mueller and Schaefer (2003) have shown that the modification to the standard $k-\varepsilon$ model to account for the effects of anisotropy does not improve the predictions. Further, the use of RST models do not improve the predictions of turbulent flow in stirred vessels compared with the standard $k-\varepsilon$ turbulence model (Montante *et al.*, 2001b). Therefore, the standard $k-\varepsilon$ model was used in the present work.

This paper reports the performance optimization of a new grid disc impeller that was developed by the present authors (Buwa *et al.*, 2006). In their previous work, the authors performed numerical simulations of the flow generated by the radial grid disc impeller and validated the predictions rigorously using LDA measurements of mean velocities and turbulent kinetic energy. In the present work, numerical simulations of the flow generated and mixing achieved by the grid disc impeller were performed using a commercial flow solver CFX 5.7 (ANSYS Inc., USA). Effects of impeller rotational speed over a wide range of impeller Reynolds numbers (180–720 rpm, $Re_I = 30\,000-120\,000$), impeller diameters ($D = T/3$ and $T/2$) and grid opening sizes (5 mm and 10 mm or $T/60$ and $T/30$, respectively) on the mixing performance per unit power consumed were investigated. The simulated mixing time and power consumption were used to evaluate the performance of the different configurations of the grid disc impeller against those of the conventionally used impellers. Simulations were also performed to evaluate the mixing performance and power consumption of a dual radial grid disc impeller.

NUMERICAL SIMULATIONS

Modelling of Rotational Motion of the Impeller

There are three different approaches extensively described in the literature to model the rotational motion of the impeller: (1) the black box approach, (2) the multiple frames of reference approach and (3) the sliding mesh approach. The black box approach [also termed as the impeller boundary condition (IBC) approach] was used in most of the earlier work on numerical simulations of fluid flow in stirred vessels. However, this approach has inherent limitations, mainly because of the fact that different flow configurations need different boundary conditions for the box surrounding the impeller that are difficult to determine *a priori* (Ranade and Joshi, 1990). In the 'multiple reference frames' (MRF) approach (Luo *et al.*, 1994), the governing equations are solved using a rotating frame of reference in the impeller region and a stationary frame of reference in the tank region. In the sliding mesh approach, a time-dependent moving and deforming grid is used to resolve the unsteady flow structures (Brucato *et al.*, 1998). However, this requires excessive computational resources to overcome the start-up flow problem when starting the flow from the rest and therefore this approach is not suitable for the design purposes. It may be noted that another method termed as the immersed boundary method (Verzicco *et al.*, 2004; Derksen and Van den Akker, 1999) has been used in the literature to treat the effect of the impeller rotation on the flow field. In this method, values of velocity are specified at points within the flow field based on the body forces arising due to the impeller geometry and motion. In the present work, we used the MRF approach. Different ways of exchanging the information at the interface between the rotor and stator regions were also analysed in the present investigations and these results are discussed in the Numerical Solution section.

Governing Equations

The numerical simulations of the flow in the stirred vessel flow generated by the grid disc impeller were carried out by solving the Reynolds-averaged mass and momentum conservation equations, which can be written as follows:

$$\frac{\partial \rho}{\partial t} + \nabla \cdot (\rho u) = 0 \tag{1}$$

$$\frac{\partial}{\partial t}(\rho u) + \nabla \cdot (\rho u u) = -\nabla P + \nabla \cdot \tau + f \tag{2}$$

where ρ denotes the fluid density, u the mean velocity, P the pressure, f the body force and τ the stress tensor, which can be written as

$$\tau = -\mu_{\text{eff}}[(\nabla u) + (\nabla u)^T] + \frac{2}{3}\mu_{\text{eff}}\delta \nabla \cdot u \tag{3}$$

Different sets of governing equations were solved in the tank and impeller regions using the stationary and rotating frames of reference, respectively. In the rotating frame of reference attached to the rotor, the momentum equations contain additional terms due to the centrifugal and Coriolis forces:

$$\left.\begin{aligned} f_r &= \rho(\omega^2 r + 2\omega u_\theta) \\ f_\theta &= \rho(-2\omega u_r) \\ f_z &= -\rho g \end{aligned}\right\} \tag{4}$$

where f_r, f_θ and f_z are the body force terms in the momentum equations for the radial, tangential and axial directions, respectively, and ω denotes rotational speed of the coordinate system.

The standard $k-\varepsilon$ model (Launder and Spalding, 1974) was used to simulate the fluid turbulence. The modelled forms of the transport equations for the turbulent kinetic energy and its dissipation rate can be written as follows:

$$\frac{\partial k}{\partial t} + \nabla \cdot (ku) = \nabla \cdot \left(\frac{\nu_t}{\sigma_k}\nabla k\right) - \varepsilon \tag{5}$$

$$\frac{\partial \varepsilon}{\partial t} + \nabla \cdot (\varepsilon u) = \nabla \cdot \left(\frac{\nu_t}{\sigma_\varepsilon}\nabla \varepsilon\right) + \frac{\varepsilon}{k}(c_{\varepsilon 1} - c_{\varepsilon 2}\varepsilon) \tag{6}$$

with the standard model constants $c_{\varepsilon 1} = 1.44$, $c_{\varepsilon 2} = 1.92$, $c_\mu = 0.09$, $\sigma_k = 1.0$ and $\sigma_\varepsilon = 1.3$ (Launder and Spalding, 1974). The momentum conservation equation was closed by calculating the effective viscosity μ_{eff} from the turbulent kinetic energy and its dissipation rate as

$$\mu_{\text{eff}} = \mu + \frac{\rho C_\mu k^2}{\varepsilon} \tag{7}$$

where μ denotes the molecular viscosity.

Vessel Geometry

A cylindrical vessel [diameter (T) = 300 mm], with four baffles (baffle width 24 mm and thickness 2 mm with no wall clearance) and a vessel height (H) to T ratio of 1, was considered for the numerical investigations [Figure 1(b)]. Three different configurations of radial grid disc impeller, as shown in Figure 2, were considered. In all configurations the diameter of the shaft was $T/37.5$ (=8 mm) and the height of grid disc impeller was 1 mm. The number of spokes in three configurations shown in Figures 2(a)–(c) was 32, 16 and 24, respectively. The effect of impeller diameter on the mixing performance of the radial grid disc impeller was investigated by using the radial grid disc impellers of diameter $T/3$ and $T/2$. Two different sizes of opening or pitch (P) of 5.25 mm and 10 mm ($\approx T/60$ and $T/30$, respectively) were investigated (see Figure 2). All simulations were performed for an impeller bottom clearance of $T/3$. In the simulations performed using dual impellers, two radial grid disc impellers (with $D = T/3$ and $P = T/30$) were located with the top and bottom clearances of $T/3$. Water at the ambient conditions was assumed to be the working fluid ($\rho = 1000\ \text{kg m}^{-3}$ and $\mu = 0.8899 \times 10^{-3}\ \text{kg m}^{-1}\ \text{s}^{-1}$). The impeller rotational speeds were varied from 180 to 720 rpm (with corresponding impeller Reynolds numbers in the range 30 000–120 000, for the impeller with $D = T/3$).

Numerical Solution

The governing equations described earlier were solved using the commercial flow solver CFX 5.7 (ANSYS Inc.). Owing to the geometrically symmetrical features of the

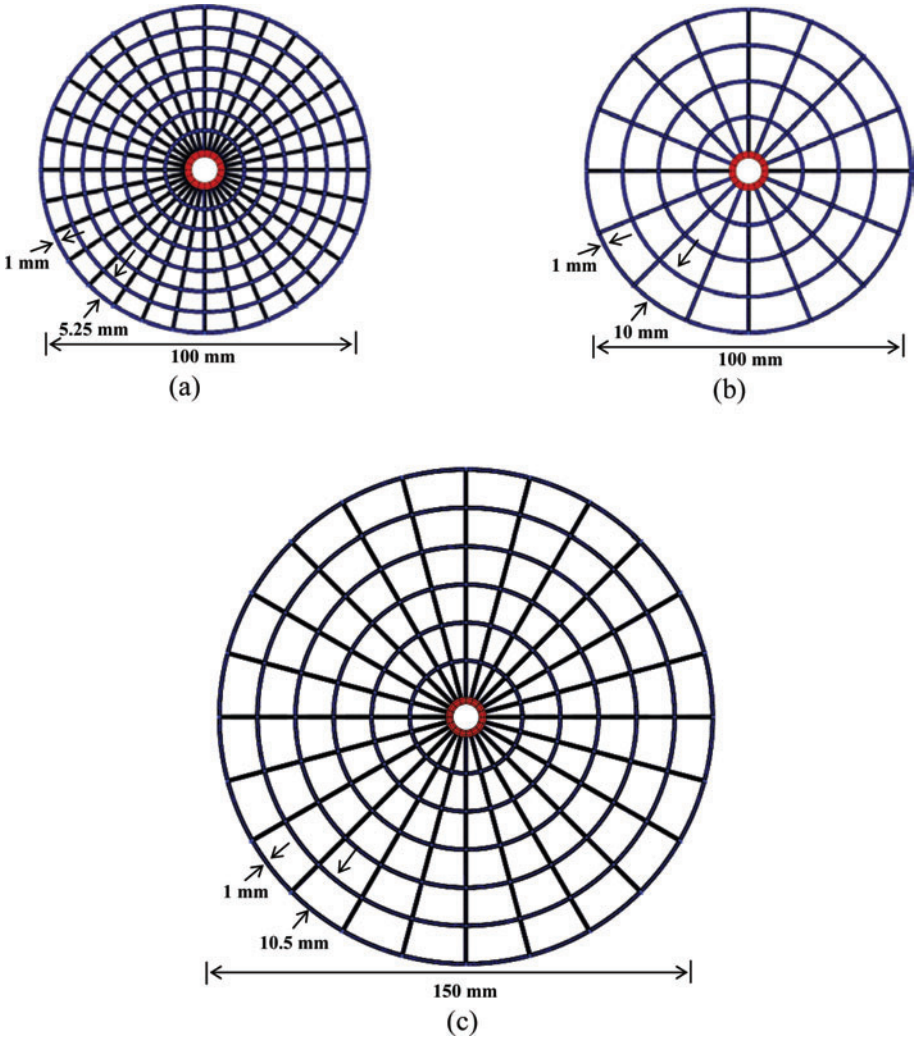


Figure 2. Different configurations of radial grid disc impellers investigated in the present work: (a) $D = 100$ mm, $P = 5.25$ mm; (b) $D = 100$ mm, $P = 10$ mm; and (c) $D = 150$ mm, $P = 10.5$ mm. This figure is available in colour via www.icheme.org/cherd.

vessel and impeller about the axis of rotation, one-quarter of the vessel was considered for the numerical simulations with the rotationally periodic boundary conditions at the corresponding faces in the impeller and tank regions [see Figure 3(a)]. The no-slip boundary condition was imposed at all the solid walls of the tank and the grid disc with the scalable wall functions. A hybrid unstructured mesh (composed of hexahedral elements in the stator region and tetrahedral elements in the rotor region) was generated using a commercial grid generation software ICEMCFD-5.0 (ANSYS Inc.), as shown in Figure 3(b) and (c). In order to resolve the flow through the impeller grid openings accurately, a sufficiently large number of cells were used in the rotating impeller region. The details of the computational grid and the extents of the impeller region used in the present numerical simulations for the single impeller ($D = 100$ mm and 150 mm) and the dual impeller ($D = 100$ mm) case are given in Table 1. Buwa *et al.* (2006) have studied the effect of grid resolution on the predicted flow field and the results are discussed in the next section.

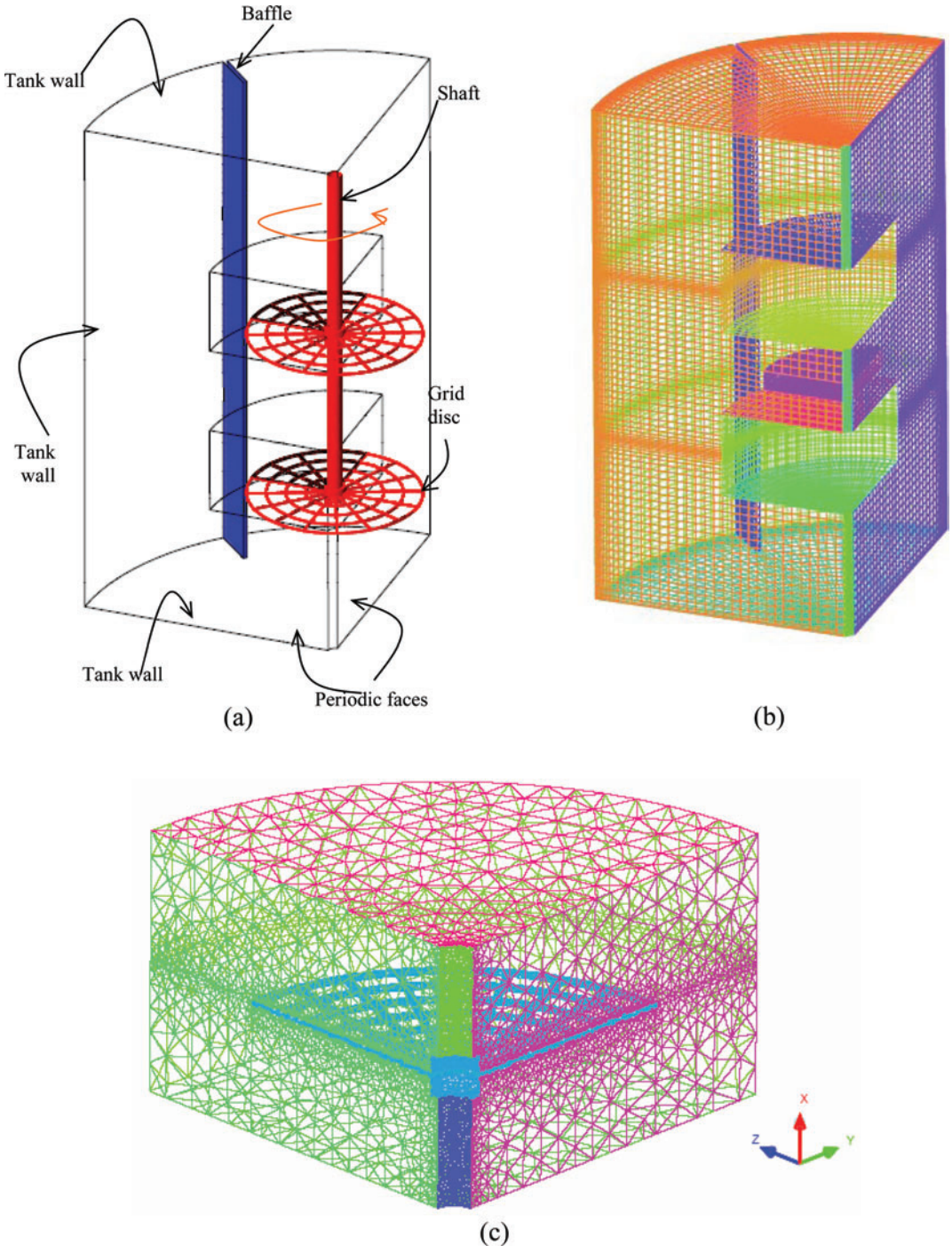


Figure 3. (a) Solution domain and the boundary conditions; (b) typical grid distribution used in the tank region; and (c) typical grid distribution used in the impeller region. This figure is available in colour via www.icheme.org/cherd.

Table 1. Details of the impeller region and computational grid used in the present work.

	Impeller region		Number of cells	
Impeller configuration	Radial direction (mm)	Axial direction (mm)	Impeller region	Tank region
Single impeller, $D = 100$ mm	$0 < r < 75$	$75 < z < 125$	97 604	97 375
Single impeller, $D = 150$ mm	$0 < r < 100$	$75 < z < 125$	194 077	101 992
Dual impeller, $D = 100$ mm	$0 < r < 75$	$75 < z < 125$	97 604	109 592
		$175 < z < 225$	97 604	

The spatial derivative terms in the governing equations described earlier were discretized using a second order accurate scheme (which reduces to first order near the discontinuities and in the free stream where the solution has little variation, see CFX 5.7 User Manual for further details). In all simulations, computations were performed until the residuals of mean velocities, pressure and turbulence quantities were $<1 \times 10^{-6}$. A typical simulation started from the previously obtained solution (for other set of parameters) using four Itanium processors in parallel took ~48 h of CPU time to achieve the converged solution.

For the MRF approach, preliminary simulations were performed to check the adequacy of different ways of exchanging the information at the interface between the stator and rotor regions. In the first approach, the flow properties were circumferentially averaged at the interface and used as the boundary condition for the outer region ('stage' approach). In the second approach, no averaging was carried out while exchanging the information ('frozen rotor' approach). We compared the results (not shown here) from both approaches ('stage' and 'frozen rotor' available in CFX-5.7) and found that the results were not much different. Therefore, the stage approach was used in all final simulations as it was considered to be physically more realistic than the frozen rotor approach.

RESULTS AND DISCUSSION

Flow Generated by the Grid Disc Impeller and Experimental Validation by Buwa *et al.* (2006)

The flow generated by the radial grid impeller ($D = 100$ mm, $P = 5.25$ mm) at an impeller rotational speed of 360 rpm (corresponding to $Re = 60\,000$) is shown in Figure 4(a). The radial flow generated by the grid disc impeller with two circulation regions can be clearly seen from the vector plot in Figure 4(a). Buwa *et al.* (2006) measured the mixing performance of this radial grid disc impeller and showed experimentally that the mixing performance of this impeller per unit power consumed was as good as that of a propeller, which is known to generate axial flow and has low power consumption. They also simulated the flow generated by such a radial grid disc impeller using the commercial flow solver CFX 5.7. The predicted mean velocity components and turbulent kinetic energy were compared with the LDA measurements. It was observed that the predicted mean velocities were in reasonably good agreement with the experiments to justify the application of the simulation method described previously to predict the performance of the grid disc impeller. Further numerical simulations were therefore performed to optimize the mixing

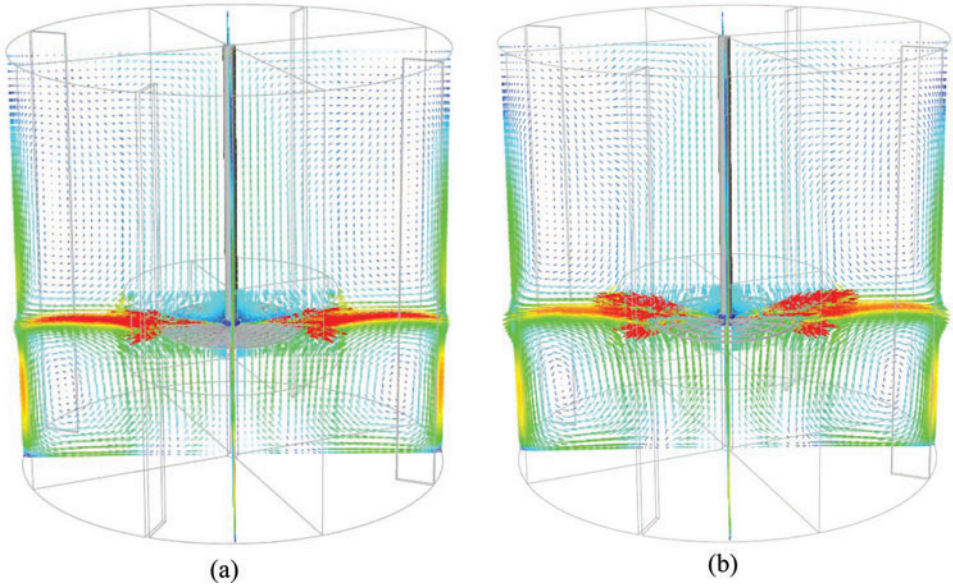


Figure 4. Predicted mean velocity flow field at a vertical plane 22.5° behind baffle in the direction of grid disc impeller rotation (anticlockwise) at 360 rpm ($Re = 60\,000$): (a) $D = 100$ mm, $P = 5.25$ mm and (b) $D = 100$ mm, $P = 10$ mm. [Blue (0 m s^{-1}) to red (0.3 m s^{-1})]. This figure is available in colour online via www.icheme.org/cherd.

performance of the grid disc impeller. In particular, the effects of the impeller grid disc opening size, impeller diameter and number of impellers on the predicted mean flow field, power consumption and mixing time were studied and the results are presented in the following sections.

Effect of Grid Opening Size and Impeller Diameter

The effect of the impeller grid opening size (P) was investigated for an impeller of 100 mm diameter and grid openings of $P = 5.25$ and 10 mm [see Figure 2(a) and (b)]. The impeller with a 5.25 mm grid opening generates strong radial flow, as shown in Figure 4(a). However, the cross flow through the grid opening was not significant. Figure 5 shows the predicted power numbers (N_P) as a function of the impeller Reynolds numbers (Re) (corresponding to the impeller rotational speeds of 180–720 rpm). Since the flow is fully developed turbulent flow for all the values of impeller Reynolds number considered, the power number is found to have a constant value of 0.72. The predicted power number was also compared with the experiments of Buwa *et al.* (2006) and it can be seen that the agreement between the predicted power number and those measured experimentally is satisfactory. It can also be seen from Figure 5 that the measured power numbers for the radial grid impeller were the same as those of the axial flow impeller, for example that of a propeller, which is known to have low power requirements. The power number of the radial flow impeller, for example, a Rushton turbine, was found to be much larger ($N_P = 6.2$) than for the grid disc impeller. It may be noted that for a comparison of the mixing performance of the various impellers, the mixing time should also be considered along with the power requirements.

The liquid-phase mixing was simulated by solving an additional Reynolds-averaged species transport equation for turbulent flow. The turbulent dispersion of the species was taken into account by the eddy viscosity obtained from the standard $k-\varepsilon$ model. The mixing simulation was started by the instantaneous addition of a tracer near the shaft slightly below the water level in the tank after a steady flow solution had been obtained. The location of the tracer injection point was the same as that in the experiments and the injected tracer volume was 0.136% of the tank volume as used in the experiments. During the mixing simulation, only the unsteady species transport equation was solved using the already converged mean flow fields.

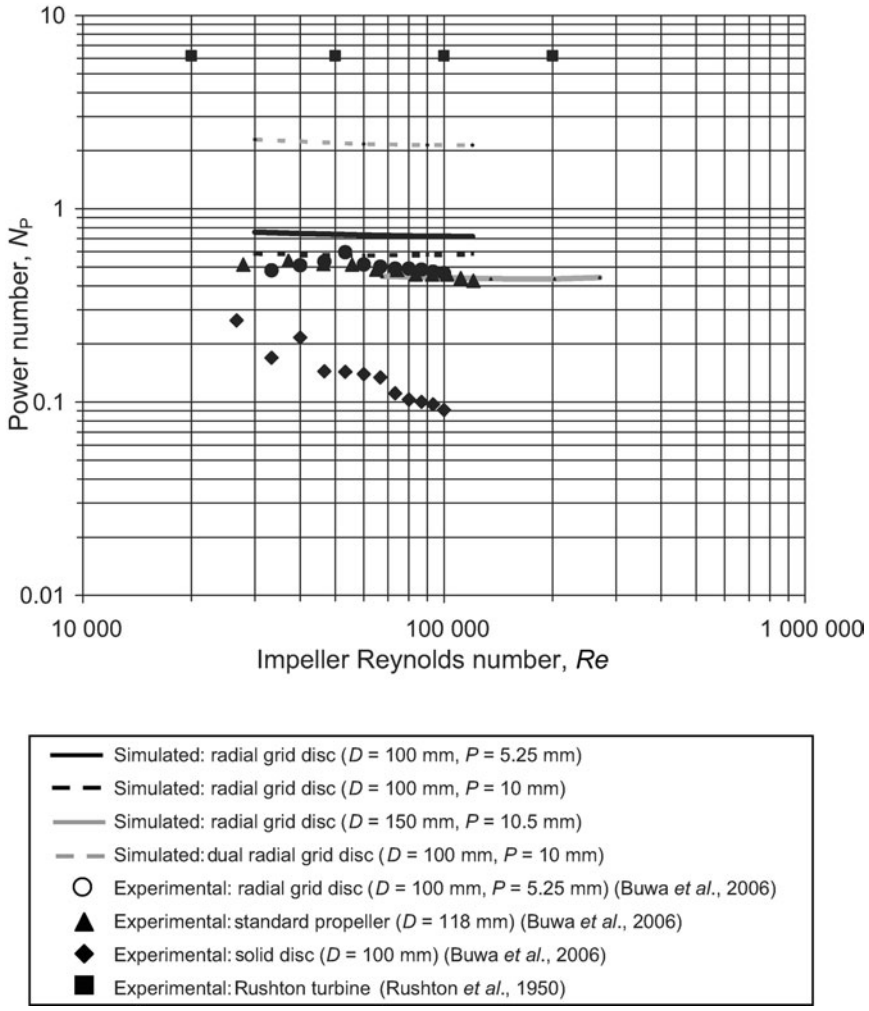


Figure 5. Variations of power number with Reynolds number for different impellers studied in the present work with that of the standard propeller and Rushton turbine.

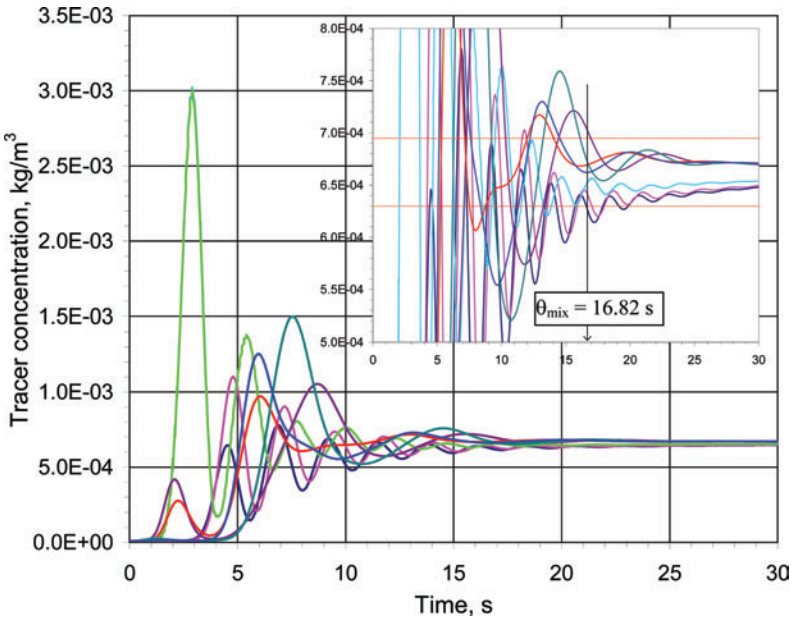


Figure 6. Predicted tracer time history monitored at different locations in the vessel (radial grid disc impeller, $D = 100$ mm, $P = 10$ mm, 360 rpm). This figure is available in colour online via www.icheme.org/cherd.

It may be noted that the mixing time values based on the tracer concentration–time history recorded at any particular location in the vessel can be sensitive to the location of the tracer monitor point and therefore may not provide the correct overall mixing time. Therefore, to avoid such a discrepancy, eight monitor points distributed over the entire solution domain were considered for the estimation of the mixing time. A typical evolution of the tracer concentrations at these locations is shown in Figure 6. The mixing time was calculated from the tracer concentration–time history recorded at each monitoring point as the time required for the tracer concentration to lie within $100 \pm 5\%$ of the final (equilibrium) tracer concentration. The average of the mixing times calculated at different monitor points was used to characterize the mixing process.

The predicted mixing time of the radial grid disc impeller ($D = 100$ mm, $P = 5.25$ mm) at different rotational speeds is shown in Figure 7. It can be seen that the predicted mixing times agree well with the measurements of Buwa *et al.* (2006). Usually, good mixing performance is achieved at the cost of high power consumption and therefore an efficient impeller is the one that has short mixing time and low power consumption. Therefore, a good method to compare the mixing performances of different impellers is to plot mixing time versus power consumption in a single plot, as shown in Figure 8. A particular impeller with the lowest performance curve in such a plot will have the best mixing performance. The corresponding predicted mixing performance of the radial disc impeller ($D = 100$ mm, $P = 5.25$ mm) as a function of the power consumed is also shown in Figure 8.

The flow generated by the radial grid disc impeller with a 10 mm grid opening is shown in Figure 4(b). A significant cross-flow through the grid opening was observed, unlike for the impeller with a 5.25 mm grid opening [see Figure 4(a)]. Such a cross flow through the impeller led to an improvement in the performance of the impeller, as shown in Figure 8. In particular, the increase in the grid opening size led to a decrease in the power number and mixing time as shown in Figures 5 and 7, respectively, for the impeller rotational speeds in the range 180–720 rpm. Since the mixing performance improved with an increase in the grid opening, we further investigated the effect of the impeller diameter on the mixing performance by considering an impeller with a diameter of 150 mm and a grid opening of 10.5 mm. A typical flow generated by this large diameter impeller ($=T/2$) is shown in Figure 9(a). Owing to the increased cross flow through the openings of the impeller with a large diameter, the mixing time is significantly reduced in comparison with that obtained by an impeller with 100 mm diameter and a 10 mm grid opening (Figure 7). However, the power numbers at different impeller Reynolds numbers for this impeller were also high as shown in Figure 5. The overall mixing performance

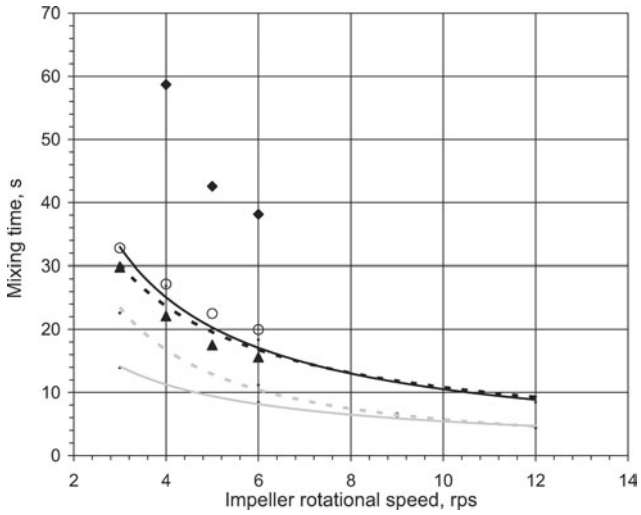


Figure 7. Comparison of measured and predicted mixing times (legend same as shown in Figure 5).

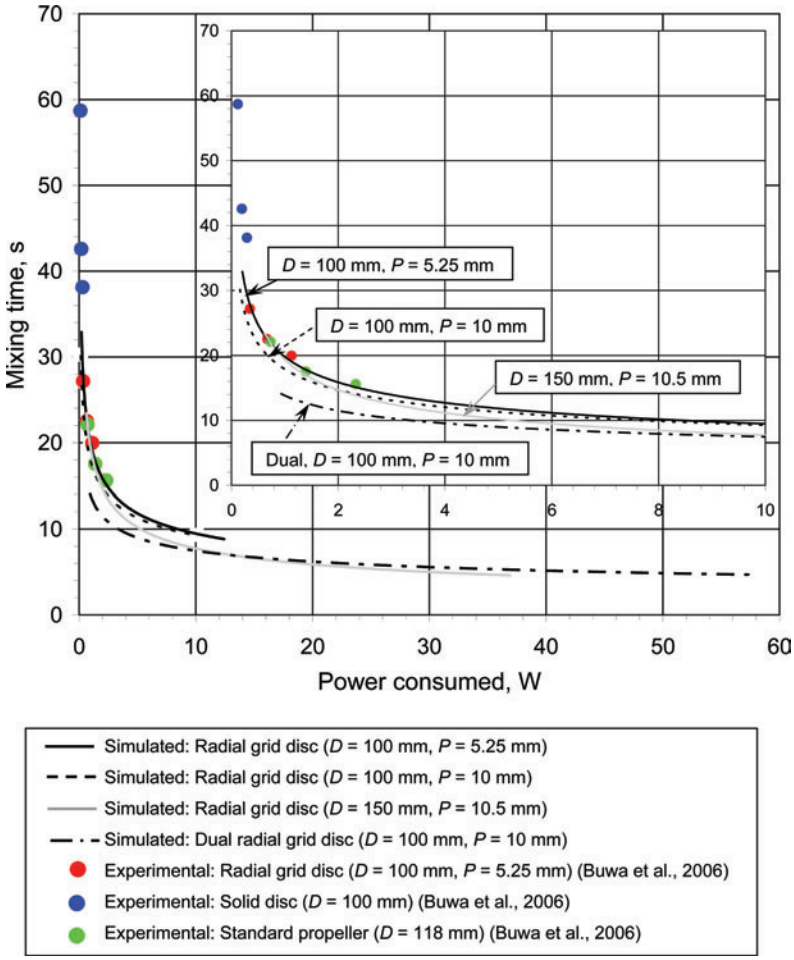


Figure 8. Mixing performance of various radial grid disc impellers. This figure is available in colour online via www.icheme.org/cherd.

per unit power consumed of the impeller with large diameter ($=T/2$) was almost the same as that of the impeller with small diameter ($=T/3$) (see Figure 8).

In order to evaluate the pumping capacity of the grid disc impeller, the pumping numbers of different grid disc impellers were computed as

$$N_Q = \frac{4\int_{z_1}^{z_2}\int_0^{\pi/4} Ru_r\, d\theta\, dz}{ND^3} \tag{8}$$

where R is the impeller radius, u_r the mean radial velocity and z_1 and z_2 the limits of integration in the axial direction. For radial flow impellers (e.g., a Rushton turbine) z_1 and z_2 are set equal to the height of the blade ($+B_w/2$ and $-B_w/2$, where B_w is the blade height). In the case of a radial grid disc impeller, although the grid thickness (corresponding to the blade height) was 1 mm, liquid was discharged through all the openings of the grid disc leading to a height of the discharge stream at $r = R$ of much more than 1 mm (see Figures 4 and 9). The z-integration limits in equation (8) were therefore set as 85–115 mm ($z/T = 0.284$–0.384, respectively) to account for the entire discharge stream generated by the grid disc impeller. Further extension of the integration height in the axial direction had negligible influence on the calculated pumping numbers. It was observed that the pumping numbers calculated for different configurations of the grid disc impellers ($D = T/2$, $T/3$ and $P = 5.25$ and 10 mm) were in the range 0.19–0.22. The pumping numbers of a Rushton turbine for fully developed turbulent flow regime are about 0.75 (Ranade, 1997). Further, the pumping numbers were also found to remain constant for the range of impeller rotational speeds considered in this work and these were not influenced by the configuration of the grid disc impeller (impeller diameter and grid disc opening).

Effect of Number of Impellers

The effect of number of impellers was also investigated by considering a dual impeller configuration. Rutherford *et al.* (1996) have reported that a dual impeller configuration with each impeller located at top and bottom clearances of $T/3$ has lower power consumption and better mixing characteristics than that of other configurations of dual impellers. Following Rutherford *et al.* (1996), we used dual grid disc impellers (each of $D = 100$ mm and $P = 10$ mm) with top and bottom clearances of $T/3$. The simulations were carried for impeller speeds in the range 180–720 rpm. A typical flow generated by a dual grid disc impeller is shown in Figure 9(b). The merged fluid streams generated by the two impellers can be clearly seen and this behavior agrees well with the characteristics of dual impellers reported in the literature (Rutherford *et al.*, 1996). The predicted power number and mixing

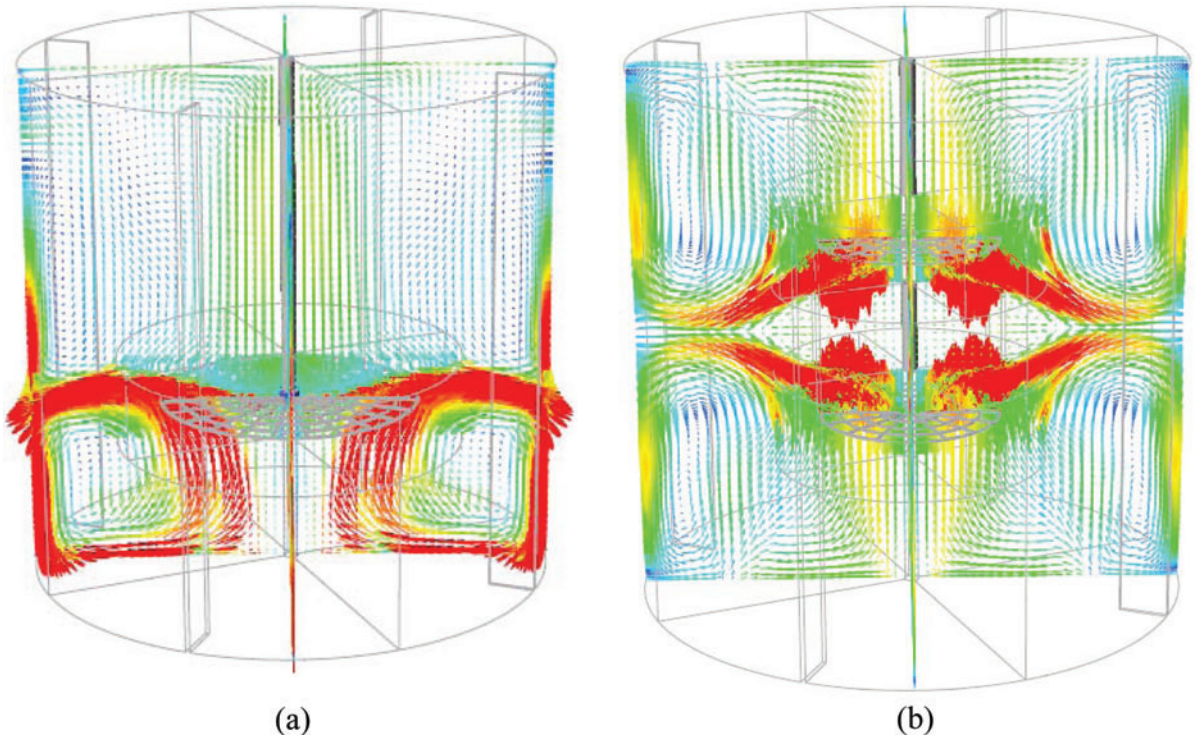


Figure 9. Predicted mean velocity flow field at 360 rpm at a vertical plane 22.5° behind baffle in the direction of impeller rotation (anticlockwise) (a) radial grid disc impeller ($D = 150$ mm, $P = 10.5$ mm, $Re = 135\,000$), (b) dual radial grid disc impeller ($D = 100$ mm, $P = 10$ mm, $Re = 60\,000$). [Blue (0 m s^{-1}) to red (0.3 m s^{-1})]. This figure is available in colour online via www.icheme.org/cherd.

time are shown in Figures 5 and 7, respectively, for the dual impeller case. Although the power requirement of the dual impeller was significantly higher than that of the corresponding single impeller case ($D = 100$ mm and $P = 10$ mm), the mixing time was significantly reduced compared with that of the later. However, the overall mixing performance per unit power consumed was significantly improved for the dual impeller case (see Figure 8) than that of all the impeller configurations investigated in the present work.

In order to understand the mixing characteristics of the dual impeller further, we analysed the tracer concentration–time history recorded at different locations in the vessel (Figure 10). The time of evolution of tracer

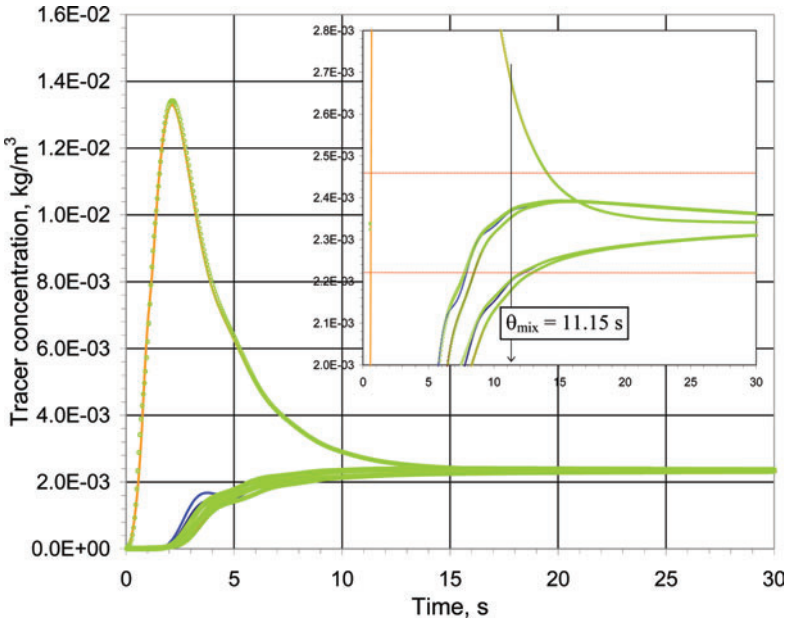


Figure 10. Predicted tracer time history monitored at different locations in the vessel (dual radial grid disc impeller, $D = 100$ mm, $P = 10$ mm, 360 rpm). This figure is available in colour online via www.icheme.org/cherd.

concentration for the single impeller ($D = 100$ mm and $P = 10$ mm) at the same rotational speed (360 rpm) is shown in Figure 6. For a dual impeller, it can be seen that the tracer is immediately dispersed owing to high turbulence, as evidenced by only one oscillation in the tracer concentration–time profiles (Figure 10). In the case of a single impeller, however, several circulations of fluid in the vessel were required for the mixing of the tracer, as evidenced by several oscillations in the tracer concentration–time profiles (Figure 6). It can be inferred from these observations that the convective mixing is dominant in a vessel with a single impeller with lower impeller rotational speeds. If the turbulence levels are higher (as in the case of a dual impeller or a single impeller with higher rotational speeds), most of the mixing is achieved by the turbulent dispersion of the tracer rather than that by the convective transfer. Further work is in progress to quantify the roles of the convective and turbulent dispersion in liquid mixing in stirred vessels.

CONCLUSIONS

The flow generated and fluid mixing achieved by a novel grid disc impeller were investigated numerically. The three-dimensional rotational turbulent mean flow generated by grid disc impeller was computed by solving the Reynolds-averaged Navier–Stokes equations. The standard $k-\varepsilon$ model along with wall functions was used to account for the fluid turbulence. The multiple frames of reference approach was used to model the impeller rotation with respect to the stationary vessel and its components. The numerical simulations were performed to optimize the mixing performance of the grid disc impeller. In particular, the effects of the impeller rotational speed, impeller grid opening size and impeller diameter were investigated. Investigations were also carried out using a dual grid disc impeller.

It was observed that the mixing performance of the grid disc impeller per unit power consumed is better than that of a propeller, which is known to have low power requirements. An increase in the grid disc openings led to a reduction in the power consumption and at the same time, a decrease in mixing time and therefore an improved overall mixing performance. Although an increase in the impeller diameter requires more power compared with a smaller diameter, its overall mixing performance per unit power consumed was better than that of the impeller with a smaller diameter. The overall mixing performance per unit power consumed of the dual impeller was the most promising of all the configurations investigated.

NOMENCLATURE

$C_{\varepsilon 1}$, $C_{\varepsilon 2}$, C_{μ}	model constants used in equations (6) and (7)
D	impeller diameter, m
f	body force term used in equation (2), kg m^{-2} s^{-2}
f_r, f_θ, f_z	body force components defined by equation (4), kg m^{-2} s^{2}
g	gravitational acceleration, m s^{-2}
H	liquid height in the tank, m
N	impeller rotational speed, rpm
N_P	power number ($=P/\rho N^3 D^5$)
N_Q	pumping number [defined by equation (8)]
P	power consumption, W
R	impeller radius, m
r	radial coordinate, m
Re	impeller Reynolds number ($= ND^2/\nu$)
t	time, s
T	tank diameter, m
u	mean velocity, m s^{-1}
z	axial coordinate, m
Greek symbols	
ρ	fluid density, kg m^{-3}
μ	fluid viscosity, kg m^{-1} s^{-1}
ν, ν_t	kinematic viscosity, m^2 s^{-1}
σ_k, σ_ε	model constants used in equations (5) and (6)
τ	stress tensor defined by equation (3)
k	turbulent kinetic energy, m^2 s^{-2}
ε	dissipation rate of the turbulent kinetic energy, m^2 s^{-3}
θ	tangential coordinate

REFERENCES

Aubin, J., Mavros, P., Fletcher, D.F., Bertrand, J. and Xuereb, C., 2001, Effect of axial agitator configuration (up-pumping, down-pumping, reverse rotation) on flow patterns generated in stirred vessels, *Chem Eng Res Des*, 79: 845–856.

Brucato, A., Ciofalo, M., Grisafi, F. and Micale, G., 1998, Numerical prediction of flow fields in baffled stirred vessels: a comparison of alternative modeling approaches, *Chem Eng Sci*, 53: 3653–3684.

Buwa, V., Dewan, A., Nassar, A.F. and Durst, F., 2006, Fluid dynamics and mixing of single phase flow in a stirred vessel with a grid disc impeller: Experimental and numerical investigations, *Chem Eng Sci*, 61: 2815–2822.

Derksen, J.J., Doelman, M.S. and Van den Akker, H.E.A., 1999, Three-dimensional LDA measurements in the impeller region of a turbulently stirred tank, *Experiments in Fluids*, 27: 522–532.

Derksen, J. and Van den Akker, H.E.A., 1999, Large eddy simulations on the flow driven by a Rushton turbine, *American Institute of Chemical Engineers Journal*, 45: 209–221.

Jenne, M. and Reuss, M., 1999, A critical assessment on the use of k−ε turbulence model for simulation of turbulent flow induced by a Rushton turbine in a baffled stirred tank reactor, *Chem Eng Sci*, 54: 3921–3941.

Jones, R.M., Harvey, A.D. and Acharya, S., 2001, Two-equation turbulence modeling for impeller stirred tanks, *ASME Journal of Fluids Engineering*, 123: 640–648.

Khopkar, A.R. Mavros, P., Ranade, V.V. and Bertrand, J., 2004, Simulation of flow generated by an axial-flow impeller: batch and continuous operation, *Chem Eng Res Des*, 82(A6): 737–751.

Kramers, H., Baars, G.M. and Knoll, W.H., 1953, A comparative study on the rate of mixing in stirred tanks, *Chem Eng Sci*, 2: 35–41.

Launder, B.E. and Spalding, D.E., 1974, The numerical computation of turbulent flows, *Computer Methods in Applied Mechanics and Engineering*, 3: 269–289.

Lee, K.C. and Yianneskis, M., 1998, Turbulence properties of impeller stream of a Rushton turbine, *American Institute of Chemical Engineers Journal*, 44: 13–24.

Li, M., White, G., Wilkinson, D. and Roberts, K.J., 2004, LDA measurements and CFD modeling of a stirred vessel with a retreat curve impeller, *Ind Eng Chem Res*, 43: 6534–6547.

Luo, J.Y., Issa, R.I. and Gosman, A.D., 1994, Prediction of impeller-induced flows in vessels using multiple frames of reference, *Institution of Chemical Engineers Symposium Series*, 136: 549–556.

Mavros, P., Mann, R., Vlaev, S.D. and Bertrand, J., 2001, Experimental visualization and CFD simulation of flow patterns induced by a novel energy saving dual-configuration impeller in stirred vessels, *Transactions of Institution of Chemical Engineers*, 79: 857–866.

Micale, G., Brucato, A., Grisafi, F. and Ciofalo, M., 1999, Prediction of flow fields in a dualimpeller stirred vessel, *American Institute of Chemical Engineers Journal*, 45: 445–464.

Montante, G., Lee, K.C., Brucato, A. and Yianneskis, M., 2001a, Experiments and predictions of the transition of the flow pattern with impeller clearance in stirred tanks, *Computers and Chemical Engineering*, 25: 729–735.

Montante, G., Lee, K.C., Brucato, A. and Yianneskis, M., 2001b, Numerical simulations of the dependency of flow pattern on impeller clearance in stirred vessels, *Chem Eng Sci*, 56: 3751–3770.

Mueller, S.E. and Schaefer, M., 2003, DNS and LES of the turbulent flow in a Rushton turbine, *Annual Meeting of GVC Working Party on CFD*, Berlin.

Nere, N.K., Patwardhan, A.W. and Joshi, J.B., 2003, Liquid phase mixing in stirred vessels: Turbulent flow regime, *Ind Eng Chem Res*, 42: 2661–2698.

Ranade, V.V. and Joshi, J.B., 1990, Flow generated by a disc turbine: Part II. Mathematical modeling and comparison with experimental data, *Transactions of Institution of Chemical Engineers*, 68(A): 34–50.

Ranade, V.V., 1997, An efficient computational model for simulating flow in stirred vessels: a case of Rushton turbine, *Chem Eng Sci*, 52: 4473–4484.

Rushton, J.H., Costich, E.W. and Everett, H.J., 1950, Power characteristics of mixing impellers—Part II. *Chem Engng Progress*, 46: 467–476.

Rutherford, K., Lee, K.C., Mahmoudi, S.M.S. and Yianneskis, M., 1996, Hydrodynamic characteristics of dual Rushton impeller stirred vessels, *American Institute of Chemical Engineers Journal*, 42: 332.

Schafer, M., Yianneskis, M., Wachter, P. and Durst, F., 1998, Trailing vortices around a 45° pitched-blade impeller, *American Institute of Chemical Engineers Journal*, 44: 1233–1246.

Verzicco, R., Iaccarino, G., Fatica, M. and Orlandi, P., 2004, Flow in an impeller-stirred tank using an immersed-boundary method, *American Institute of Chemical Engineers Journal*, 50: 1109–1118.

ACKNOWLEDGEMENTS

A.D. and V.B. gratefully acknowledge the Alexander von Humboldt Foundation and Bavarian Science Foundation, respectively, for their research fellowships. These allowed this cooperative research work to be performed at LSTM-Erlangen.

The manuscript was received 2 November 2005 and accepted for publication after revision 30 March 2006.